THE JOURNAL OF BIOLOGICAL CHEMISTRY
Vol. 275, No. 45, Issue of November 10, pp. 35311–35319, 2000

Printed in U.S.A.

Functional Analysis of the Terminase Large Subunit, G2P, of *Bacillus subtilis* Bacteriophage SPP1*

Received for publication, May 19, 2000, and in revised form, July 14, 2000
Published, JBC Papers in Press, August 4, 2000, DOI 10.1074/jbc.M004309200

Aranzazu Gual, Ana G. Camacho‡, and Juan C. Alonso§

From the Departamento de Biotecnología Microbiana, Centro Nacional de Biotecnología, Consejo Superior de Investigaciones Científicas, Campus Universidad Autónoma de Madrid, Cantoblanco, Madrid 28049, Spain

The terminase of bacteriophage SPP1, constituted by a large (G2P) and a small (G*1*P) subunit, is essential for the initiation of DNA packaging. A hexa-histidine G2P (H6-G2P), which is functional *in vivo*, possesses endonuclease, ATPase, and double-stranded DNA binding activities. H6-G2P introduces a cut with preference at the 5′-RCGG↓CW-3′ sequence. Distamycin A, which is a minor groove binder that mimics the architectural structure generated by G*1*P at *pac*, enhances the specific cut at both *bona fide* 5′-CTATTGCGG↓C-3′ sequences within *pac*C of SPP1 and SF6 phages. H6-G2P hydrolyzes rATP or dATP to the corresponding rADP or dADP and P_i. H6-G2P interacts with two discrete G*1*P domains (I and II). Full-length G*1*P and G*1*PΔN62 (lacking domain I) stimulate 3.5- and 1.9-fold, respectively, the ATPase activity of H6-G2P. The results presented suggest that a DNA structure, artificially promoted by distamycin A or facilitated by the assembly of G*1*P at *pac*L and/or *pac*R, stimulates H6-G2P cleavage at both target sites within *pac*C. In the presence of two G*1*P decamers per H6-G2P monomer, the H6-G2P endonuclease is repressed, and the ATPase activity stimulated. Based on these results, we propose a model that can account for the role of terminase in headful packaging.

Initiation of packaging of double-stranded viral DNA (dsDNA)[1] involves the specific interaction of the prohead with viral DNA in a process mediated by a phage-encoded terminase protein (1–4). The terminase enzymes are usually hetero-oligomers composed of a small and a large subunit. The role of the terminase small subunit is to specifically recognize the packaging initiation site (*cos* or *pac*) and to form a nucleoprotein structure that helps to position the terminase large subunit to cleave at the *pac* or *cos* site (1–6). Two general principles for packaging of concatemeric DNA into a virus head have been proposed. The first implies a site-specific packaging that shows some constraint in DNA size, in which the recognition sequence (termed *cos* in phage λ) plays an important role in initiation and termination of packaging. This packaging process is well-characterized in coliphages λ, T3, and T7 (1–6). The second principle implies headful packaging, in which the packaging initiates at a specific site (termed *pac* in phage SPP1) but with the capacity of the prohead playing a predominant role in the termination step. Within the poorly characterized headful packaging mechanism, phages P1, P22, T4, and SPP1 are included (1, 3, 7).

The terminase enzyme of *Bacillus subtilis* phages SPP1 and SF6 is composed of a small (G*1*P) and a large (G2P) subunit (8). The terminase initiates unidirectional DNA packaging from a concatemeric DNA substrate by binding to *pac* DNA, introducing a 1-bp staggered cut, within the 83-bp *pac*C subsite, and encapsidating the DNA from the cleaved end into an empty prohead until no more DNA can be inserted (headful) (8–11). DNA packaging terminates when the DNA inside the prohead is separated from the concatemer by a cutting process (headful cut). The headful cleavage generates a new end that serves as the starting point for the second round of DNA packaging. The *pac*C cut is precise, and the headful cut is imprecise and could be spread over a 2.5-kb region of DNA (8, 9, 12, 13).

SPP1 and SF6 wt G*1*P are 184 and 151 residues long, respectively, and share 71% identity clustered in three discrete regions (domains I, II, and III) (14, 15). Within domain I lies the B-type nucleotide-binding motif, the DNA-binding motif, and a G*1*P:G2P interacting region, and within domain II lies the A-type putative phosphate-binding loop (A*XXXX*GK(L/A)), the G*1*P:G*1*P interacting domain, and a G*1*P:G2P interacting region (11, 14, 15). No apparent biological role can be assigned to domain III and the extended SPP1 G*1*P C-terminal region (see Refs. 14–16). G*1*P, which is unable to cleave DNA, binds but does not hydrolyze ATP (14, 15).

The SPP1 and SF6 G*1*P (native molecular masses of ~200 and ~170 kDa, respectively) consist of a specific ring containing 10 monomers of G*1*P (11).[2] A comparable ring-like structure was also observed in the terminase small subunit, gp16, of phage T4 (17). G*1*P, which is an abundant protein, binds cooperatively to two discrete (*pac*L (non-encapsidated left DNA end) and *pac*R (the encapsidated right DNA end)) subsites and holds the two binding sites together in a DNA loop of about 20 turns of the DNA helix (11, 14–16).

The SPP1 and SF6 G2P, which has a predicted molecular mass of 48,840 kDa and is a long product of 422 residues, contains a putative B-type nucleotide-binding motif preceded by hydrophobic amino acids between residues 106 and 114. An A-type NTP-binding loop (see Ref. 18), however, was not found in the G2P protein (8).[3] The presence of a histidine-rich metal-

* This work was supported in part by grants from DGCICYT (PB 96-0817) and from CEYCCAM (08.3/0028/98) (to J. C. A.). The costs of publication of this article were defrayed in part by the payment of page charges. This article must therefore be hereby marked "*advertisement*" in accordance with 18 U.S.C. Section 1734 solely to indicate this fact.
‡ Recipient of a fellowship of the CEYCCAM (0381/1999).
§ To whom correspondence should be addressed. Tel.: 34-91585-4546; Fax: 34-91585-4506; E-mail: jcalonso@cnb.uam.es.
[1] The abbreviations used are: dsDNA, double-stranded DNA; ssDNA, single-stranded DNA; Dis, distamycin A; DTE, dithioerythreitol; EMSA, electrophoretic mobility shift assay; G*X*P, gene *X* product; G*1*PΔN62, a deletion mutant of G*1*P lacking the N-terminal 62 amino acids; G*1*PΔC136, a deletion mutant of G*1*P lacking the C-terminal 47 amino acids; G*1*PΔC55, a deletion mutant of G*1*P containing residues 1–54; G*1*PΔN64-C141, a deletion mutant of G*1*P containing residues 65–141; H6-G2P, a G2P containing a hexa-histidine at the N terminus of the protein; K_{app}, apparent binding constant; PAGE, polyacrylamide gel electrophoresis; wt, wild type.

[2] A. Gual, A. G. Camacho, and J. C. Alonso, unpublished results.
[3] S. Chai and J. C. Alonso, unpublished.

binding motif, identified in the terminase large subunit of phages λ, T3, T7, and T4, and a leucine zipper region are not obvious from the primary sequence of SPP1 and SF6 G2P (8).

We have previously observed that a plasmid-borne SPP1 H6-G2P fully complements the growth defect of different SPP1 conditional lethal mutants in gene *2* (15). The results presented here provide the first evidence that the SPP1 terminase large subunit, in a DNA structure-dependent manner, introduces double strand nicks within both target sites within *pac*C. The available information suggested that the roles of G*1*P in the holoenzyme is to promote initiation of headful packaging by forming a nucleoprotein structure (8, 11) that helps to position G2P to cleave at both cognate sites, to impose directionally to DNA packaging, and to modulate DNA translocation.

EXPERIMENTAL PROCEDURES

Materials

Bacterial Strains and Plasmids—Escherichia coli strain BL21(DE3) was described previously (19). pUC18 was used as a vehicle of our constructs, because it does not contain any supercoiling-dependent structure (20). Plasmids pBT115, pBT419, and pBT363 (14); pCB191 and pCB53 (15); and pQE10 and pQE9 (Qiagen) have been described previously. Plasmids pCB236, pCB220, and pCB231, containing G*1*PΔN62, G*1*PN64-C141, and G*1*PΔC55, respectively, were constructed by fusing the indicated DNA sequence of G*1*P to the last His codon of the His-Tag pQE vector.

Enzymes and Reagents—Ultrapure acrylamide was purchased from Serva; molecular weight markers were from Bio-Rad; rifampicin was from BioChemika; DTE and proteinase K were from Sigma; trizma base was from Biomedicals, Inc.; isopropyl-1-thio-β-D-galactopyranoside was from Calbiochem; and DNA restriction and modification enzymes, phenylmethylsulfonyl fluoride, poly(dC), and poly[d(I-C)] were purchased from Roche Molecular Biochemicals. All were used as recommended by the suppliers. All chemicals used were of reagent grade, and solutions were made in quartz-distilled H_2O. [α-^{32}P]rNTP, [α-^{32}P]dNTP, or [γ-^{32}P]ATP were from Amersham Pharmacia Biotech.

Methods

DNA Manipulations—Covalently closed circular plasmid DNA was purified by using the SDS lysis method (21), followed by purification on a cesium chloride-EtBr gradient. Gel-purified DNA fragments were end-labeled by filling in the restriction site with the large fragment of DNA polymerase I in the presence of dTTP, dCTP, dGTP, and [α-^{32}P]dATP.

Analytical and preparative gel electrophoreses of plasmid DNAs and restriction fragments were carried out either in 0.8% (w/v) agarose/Tris-acetate-EDTA/EtBr horizontal slab gels or on 6% (w/v) urea/polyacrylamide/Tris-borate gels.

The concentration of DNA was determined using molar extinction coefficients of 6500 $M^{-1} \times cm^{-1}$ at 260 nm. DNA was expressed as moles of DNA molecules.

Protein Purification—SPP1 wt G*1*P and the truncated G*1*P products either lacking the first 62 residues (G*1*PΔ62 (formerly termed G*1*P*)) or the last 48 residues (G*1*PΔC136 (formerly termed Chi1)) were purified as described previously (14). *B. subtilis* chromatin-associated protein Hbsu was purified as previous described (22). G*1*PΔN55, G*1*PN64-C141, and H6-G2P were purified from BL21(DE3) cells carrying plasmids pCB231, pCB220, and pCB191, respectively, after induction with isopropyl-1-thio-β-D-galactopyranoside (1 mM). After a 30-min induction, rifampicin was added to a final concentration of 200 μg/ml. Cells were harvested by centrifugation 90 min after rifampicin addition, and the pellets were frozen at −20 °C. For the purification procedure, the pellet was thawed, resuspended in buffer A (50 mM Tris-HCl, pH 7.5, 10 mM $MgCl_2$, 2 mM DTE, 0.2 mM phenylmethylsulfonyl fluoride, 5% glycerol) containing 50 mM NaCl, and lysed with a French press. The crude extract was centrifuged at 12,000 × *g* for 30 min, and the supernatant was used for a posterior purification using a Hitrap nickel-cheating column according to the manufacturer's instructions (Amersham Pharmacia Biotech).

The molar extinction coefficient for the different proteins was calculated as described by Gill and von Hippel (23). Protein concentration was determined by UV absorbance, using the corresponding molar extinction coefficients at 280 nm. Spectra were recorded on a 4054 UV-visible spectrophotometer LKB Biochrom Ultrospec Plus. The wt G*1*P, G*1*PΔ62, and G*1*PΔC136 concentrations are expressed as moles of protein decamers, whereas the H6-G*1*PΔN55, H6-G*1*PN64-C141, and H6-G2P concentrations are expressed as moles of protein monomers.

Protein Manipulations—The native molecular mass of G2P was determined by gel filtration fast protein liquid chromatography using a Superose 12 HR 10/30 column (Amersham Pharmacia Biotech). Chromatography was carried out in buffer C (50 nM Tris-HCl, pH 7.5, 100 mM NaCl, and 5% glycerol) at 4 °C with a flow rate of 0.1 ml/min, and the A_{280} was measured. G2P (200 μg) was applied onto the column. A standard curve of K_{av} *versus* $\log_{10}$ of relative mobility was determined as recommended by Amersham Pharmacia Biotech. Protein standards were obtained from the manufacturer (ribonuclease A, 13.7 kDa; chymotrypsinogen A, 25 kDa; ovalbumin, 43 kDa; bovine serum albumin, 67 kDa; aldolase, 158 kDa; and catalase, 232 kDa).

For protein cross-linking, the pure proteins were incubated in the presence or absence of 0.04% glutaraldehyde at room temperature in buffer D (60 mM Na_2HPO_4, pH 7.2, 30 mM $MgCl_2$, and 1.5 mM DTE), containing either 25 or 100 mM NaCl. Aliquots were collected at different times, and the reactions were stopped by precipitating the proteins with 25% (w/v) trichloroacetic acid, followed by two washing steps with acetone. The pellets were dissolved in loading buffer and loaded in a 7–15% SDS-PAGE.

Electrophoretic Mobility Shift Assay—The DNA fragment used to analyze the binding of H6-G2P to DNA through EMSA was the SPP1 242-bp [α^{32}P]*Xho*II-*Hin*fI (containing part of *pac*L, *pac*C, and *pac*R sites, coordinates 157–399) from plasmid pCB363. The end-labeled DNA (1 nM) was incubated with increasing concentrations of H6-G2P in buffer B (50 mM Tris-HCl, pH 7.8, 50 mM NaCl, 2 mM DTE, 5% glycerol), containing 10 mM $CaCl_2$ (in a 20-μl reaction) for 30 min at 37 °C. When indicated, increased concentrations of poly[d(I-C)] (nonspecific) or cold SPP1 242-bp *Xho*II-*Hin*fI DNA fragment (specific) were added as competitor DNA. The reaction was stopped (by the addition of 3 μl of loading buffer (50 mM Tris-HCl, pH 7.8, glycerol 30%, bromphenol blue 0.25%, xylene cyanol 0.25%), immediately loaded onto a 1× TAE, and separated in a 4% non-denaturing PAGE. Gels were run for 3 h at 150 V and room temperature and dried prior to autoradiography.

Endonuclease Activity Assay—Supercoiled pBT363 DNA containing the SPP1 *pac* site (10 nM) was incubated with H6-G2P (20 nM) in buffer B containing 10 mM $MgCl_2$, at 37 °C for a variable time. The reaction was stopped by addition of 2 μl of loading buffer containing 0.4 M EDTA, and the resultant products were then separated in 0.8% agarose gel.

The SPP1 242-bp *Xho*II-*Hin*fI DNA fragment obtained as a 320-bp *Eco*RI-*Pst*I DNA segment from plasmid pBT363 or the SF6 233-bp *Ear*I-*Hin*fI (coordinates 223–456) obtained as a 311-bp *Eco*RI-*Pst*I DNA segment were end-labeled at the top strand. The radiolabeled DNA (1 nM) was preincubated with Dis (1 or 100 μM) in buffer B, containing 10 mM $MgCl_2$ for 20 min at 37 °C, and then incubated with H6-G2P (5–40 nM) for 60 min at 37 °C. the reaction was stopped by addition of 2 μl of loading buffer, containing 0.4 M EDTA, and the resultant products were separated in 6% denaturing PAGE. Autoradiographs of the dried gel were subsequently taken.

The SPP1 399-bp *Hpa*II-*Hin*fI DNA fragment from plasmid pCB53 was end-labeled at the bottom strand. The radiolabeled DNA (1 nM) was preincubated with increasing concentrations of Dis (1–100 μM) in buffer B, containing 10 mM $MgCl_2$ for 20 min at 37 °C, and then incubated with G2P (20 nM) for 60 min at 37 °C. The reaction was stopped by addition of 2 μl of loading buffer containing 0.4 M EDTA, and the resultant products were separated on a 6% non-denaturing PAGE. Autoradiographs of the dried gel were subsequently taken.

ATPase Activity Measurement—The ATPase standard reactions were incubated in buffer B containing 10 mM $MgCl_2$ in a final volume of 20 μl. The reactions were initiated by addition of the substrate after a preincubation of 5 min at 37 °C and allowed to proceed for 15 min more at the same temperature. ATPase activity was determined by measuring the amount of phosphate set free upon hydrolysis as described previously (24). Initial velocity studies were performed using 20 nM H6-G2P and an ATP concentration range of 0.5 μM to 10 mM (10–0.05 μCi/nmol). The initial velocity of ATP hydrolysis was determined within the linear range of each reaction, and the kinetic constants were determined by non-linear regression analysis of the experimental data using the KaleidaGraph version 3.0.2 software program (Abelbeck).

dNTP or rNTP hydrolysis reactions (30 μl) were performed in buffer B, containing 10 mM $MgCl_2$ and 400 μM dNTP (with 2 nM [α-^{32}P]dNTP) or rNTP (with 2 nM [α-^{32}P]rNTP), 150 μM poly(dC), and 20 nM of H6-G2P, for 15 min at 37 °C. Products were separated by chromatography on polyethyleneimine-cellulose as described by Scott *et al*. (25), and the formation of [α-^{32}P]dNDP or [α-^{32}P]rNDP was visualized by autoradiography and quantified by using the Molecular Imager and Molecular Analyst software package version 2.1 (Bio-Rad).

RESULTS

H6-G2P, G1P, and G1P Derivatives: Purification and Activities—SPP1 20-kDa wt G*1*P (predicted molecular mass 20.7 kDa), G*1*P variants with deletions at its N-terminal (13-kDa G*1*PΔN62) or C-terminal moiety (15-kDa G*1*PΔC136) (14) or isolated G*1*P domains (7-kDa H6-G*1*PΔC55 and 9-kDa H6-G*1*PN64-C141) (15) and the 49-kDa H6-G2P (predicted molecular mass 49.7 (H6, 0.9 + G2P, 48.8) kDa) were purified from the *E. coli* BL21(DE3) strain bearing a plasmid-borne SPP1 gene *1*, gene 1ΔC136, His-tagged domain I or domain II of gene *1*, or His-tagged gene *2* as described previously (14, 15). The purified polypeptides (G*1*P, G*1*PΔC136, G*1*PΔN62, H6-G*1*PΔC55, H6-G*1*PN64-C141, and H6-G2P) were more than 99% pure, as judged by SDS-PAGE (data not shown). N-terminal protein sequence analysis of the first 10 N-terminal residues of the purified proteins were in full agreement with the amino acid sequence deduced from the nucleotide sequences.

Previously, it has been shown that G*1*P and G*1*PΔC136 specifically bind dsDNA and are not able to hydrolyze ATP (11, 14, 15). G*1*PΔN62, H6-G*1*PΔC55, and H6-G*1*PN64-C141 do not bind DNA or hydrolyze ATP (14, 15, data not shown). The abilities of H6-G2P to act as dsDNA nuclease (exo- or endonuclease), ATPase in the presence or absence of ssDNA or dsDNA, and DNA helicase and to bind to dsDNA or ssDNA were assayed. As shown below H6-G2P possesses an endonuclease and a modest ATPase and is able to bind dsDNA. All these activities co-purified in a Ni-agarose column with H6-G2P and exhibited the same kinetics of heat inactivation (data not shown). Furthermore, such activities were not observed when the same protocol and a Ni-agarose column was used to purify proteins from BL21(DE3) plasmid-free strain (data not shown).

H6-G2P Binds in a Sequence-independent Manner to Linear DNA—EMSA had indicated that the highly purified H6-G2P interacts with a linear intrinsically curved 320-bp DNA (1 nM) fragment (containing the SPP1 242-bp *Xho*II-*Hin*fI (part of *pac*L, *pac*C, and *pac*R sites) from plasmid pCB363), provided that a divalent cation (*e.g.* Mg^{2+}, Ca^{2+}) is present in the reaction mixture. In the presence of Mg^{2+}, the DNA substrate is hydrolyzed (see below), thus we performed the experiment in buffer containing 10 mM $CaCl_2$. The protein·DNA complex was separated in a 4% non-denaturing PAGE. The 320-bp DNA segment, which migrates as a 520-bp fragment, is intrinsically curved (11). Two discrete H6-G2P·DNA complexes (CI and CII) were seen on addition of 20 and 40 nM (in monomers) of H6-G2P (Fig. 1, *lanes 5* and *4*). A slowly migrating form (CIII) and material that did not enter in the gel was observed in the presence of 80 and 160 nM of H6-G2P (Fig. 1, *lanes 3* and *2*). The K_{app} of the H6-G2P·DNA complex was estimated to be ~35 nM at pH 7.8 and 37 °C. When the H6-G2P was present in limiting amounts (35 nM), the addition of 5-fold excess of a nonspecific poly[d(I-C)] DNA fully competed for the formation of H6-G2P·*pac* DNA complex (data not shown). Furthermore, when non-curved DNA was used the H6-G2P·DNA complex did not enter in the gel (data not shown). It is likely, therefore, that H6-G2P binds curved dsDNA with low sequence specificity.

H6-G2P Exhibits a pac-independent Endonucleolytic Activity—The supercoiled (form I) pBT363-borne *pac* site, containing a small amount (<10%) of relaxed circular DNA (form II), was incubated with a fixed amount of H6-G2P for varying times (Fig. 2). The resulting products were separated in a 0.8% agarose gel (Fig. 2). At early times of incubation (Fig. 2, *lanes 2–4*) ~20% of form I DNA was converted to form II DNA, with a small fraction as form III DNA. The H6-G2P nicking of both DNA strands was uncoupled. At later times the reaction seemed to be saturated (Fig. 2, *lanes 6–12*), because no further conversion of form I DNA into form II, then into form III, was

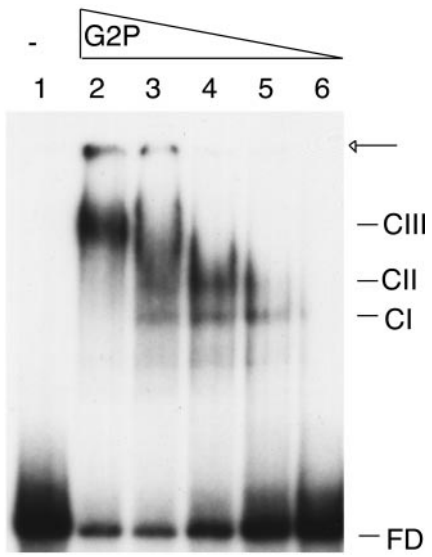

FIG. 1. **Binding of H6-G2P to linear DNA.** The α-^{32}P-labeled, 320-bp DNA fragment (1 nM) containing the SPP1 242-bp *Xho*II-*Hin*fI segment (part of *pac*L, *pac*C, and *pac*R subsites) was incubated with increasing concentrations of H6-G2P (10, 20, 40, 80, and 160 nM, *lanes 2–6*) in buffer B containing 10 mM $CaCl_2$ and analyzed by non-denaturing PAGE and autoradiography. The migration of the DNA without protein added is shown in *lane 1*. The H6-G2P·DNA complexes CI, CII, and CIII, the free-DNA (*FD*), and the DNA retained in the well (*arrow*) are denoted.

observed. A fine mapping of *pac*-containing form II DNA revealed that H6-G2P introduced many discrete endonucleolytic nicks (data not shown). Under these experimental conditions, we were not able to identify a specific cut at *pac*C. Similar results were obtained when the pUC18 DNA control was used (data not shown).

A time courses for cleavage using various concentrations of H6-G2P (80–240 nM) at a constant concentration of pBT363 DNA revealed that, at high enzyme/DNA ratios, the data are biphasic and yield a fast and slow phase of the reaction. A reduction in the enzyme concentration not only resulted in the complete disappearance of the fast rate but also substantially limited the extent of nicking (cleaving) of pBT363 DNA (data not shown). These data suggested that the reaction did not have a catalytic turnover.

No H6-G2P nuclease activity was seen in the absence of Mg^{2+} or in the presence of a 2-fold excess of EDTA with respect to the metal ion. Varying the $MgCl_2$ concentration from 0.5 to 20 mM revealed a similar pattern of cleavage by H6-G2P. Increasing concentrations of Mg^{2+} correlated with an increasing endonucleolytic activity of H6-G2P with an optimum at ~10 mM. Mn^{2+} partially replaced Mg^{2+} (an optimal concentration gave ~50% of the activity observed with Mg^{2+}), but when Ca^{2+} or Zn^{2+} was used no H6-G2P endonuclease activity was observed.

The presence of a nucleotide cofactor (0.1–1 mM ATP), which exerts a negative effect in H6-G2P endonuclease activity, did not increase the cleavage specificity of H6-G2P (data not shown).

The endonuclease activity exhibited a relatively narrow pH optimum, which was maximal at pH 7.8. The activity decreased rapidly below pH 7.0 and above pH 8.5. Increasing concentrations of NaCl correlated with an increasing endonucleolytic activity of H6-G2P until an optimum was reached at ~50 mM, with a sharp decrease beyond 120 mM NaCl.

H6-G2P Introduces Many Discrete Cuts on pac-containing DNA—The SPP1 *pac*C subsite contains two directly oriented Box b repeats (10-bp in length) (Fig. 3). DNA encapsidation

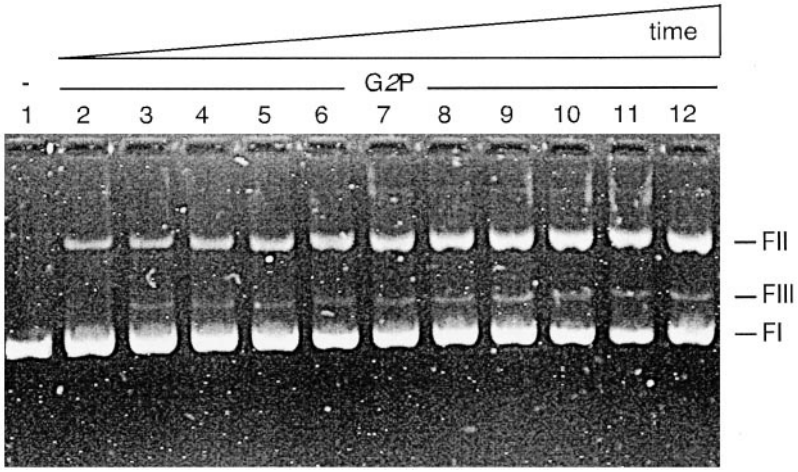

FIG. 2. **Relaxation of *pac*C-containing form I DNA by H6-G2P.** Supercoiled pBT363 (10 nM in molecules) was incubated with 5 nM H6-G2P in buffer B containing 10 mM $MgCl_2$ during the indicated time (*t*) (5, 10, 20, 30, 45, 60, 75, 90, 105, 120, and 135 min, *lanes 2–12*) at 37 °C in a final volume of 20 μl. The reactions were terminated by the addition of EDTA, and the samples were eletrophoresed on a 0.8% agarose gel run in TBE buffer. The gels were stained with EtBr and photographed. *Lane 1*, form I DNA without protein added.

initiates upon terminase cleavage at the Box b site proximal to the *pac*R subsite (8, 9, Fig. 3*A*). Hence, terminase has to discriminate between the two Box b sites at the 83-bp *pac*C subsite and to introduce a 1-bp staggered cut within one of them (5′-CTATTGCG(G ↓ C-3′) (8–10, Fig. 3*B*). On the basis of genome organization and sequence identity, we predict that the SF6 terminase upon recognition of *pac*L (non-encapsidated) and *pac*R (encapsidated end) directs the terminase large subunit toward *pac*C (Fig. 3). To initiate unidirectional encapsidation, terminase introduces a double strand cleavage within the 13-bp Box b site (5′-GCTATTGgGGG ↓ CAG-3′) proximal to *pac*R (9, see Fig. 3). Alternatively, terminase cleaves both Box b sites, but by an uncharacterized mechanism only, the cut at the Box b proximal at *pac*R is used as a substrate for *in vivo* DNA encapsidation. Previously, Chai *et al.* (8) have shown that the *pac* DNA end that is not the substrate for encapsidation is nucleolytically degraded, and such effect is independent of the major host-encoded nuclease (Exo V enzyme).

The SPP1 or SF6 *pac*C subsite located on a 242-bp *Xho*II-*Hin*fI DNA fragment (coordinates 157–399 of SPP1, obtained as a 320-bp *Eco*RI-*Pst*I DNA segment from pBT363) or on a 233-bp *Ear*I-*Hin*fI (coordinates 223–456 of SF6, obtained as a 311-bp *Eco*RI-*Pst*I DNA segment from pCB53) was used for *in vitro* cleavage assays (see Ref. 8).

In the absence of H6-G2P, three faint DNA bands (denoted by *arrows* in Fig. 4*A*) were reproducibly observed. The 320-bp *Eco*RI-*Pst*I SPP1 DNA segment or the 311-bp *Eco*RI-*Pst*I SF6 DNA segment (1 nM), labeled at the top strand, was incubated with increasing concentrations of H6-G2P (5–40 nM) in buffer B containing 10 mM $MgCl_2$, for 60 min at 37 °C, and the resulting products were then separated in 6% denaturing PAGE (Fig. 4*A*, data not shown). The endonuclease activity of the enzyme seems to be stoichiometric rather than catalytic. Six major SF6 ssDNA fragments (denoted *Z*, *Y*, *3*, *4*, *2*, and *1*, see Fig. 3) and many minor discrete ssDNA segments were observed (Fig. 4*A*). A fine mapping of SF6 *pac*-containing DNA revealed that the end of two of those fragments map outside (*Z*, *Y*) and four inside (*3*, *4*, *2*, and *1*) *pac*C (Fig. 3*B*). The fragments 1 and 2 end within the two Box b sites. The addition of a nucleotide cofactor seems to exert a negative rather than a stimulatory effect in H6-G2P nuclease activity (see below). Similar results were obtained when SPP1 *pac* DNA was used, except that here only four major DNA fragments (*Y* and *4* are missing) were observed (see Fig. 3*B*).

A nucleotide sequence analysis of H6-G2P-generated DNA ends revealed that the enzyme introduces, with certain preference, a nick in the top strand within the 5′-RCGG ↓ CW-3′ nucleotide sequence (5′-acga ↓ ca-3′ (*Z*) 5′-aacg ↓ ct-3′ (*Y*), 5′-GCCG ↓ CT-3′ (*3*), 5′-GCGG ↓ CA-3′ (*2*), 5′-TCCG ↓ C-3′ (*4*), and 5′-GGGG ↓ CA-3′ (*1*)) (see Fig. 3*B*). A low amount of the DNA segments ending at the 3 and 4 sites were also observed in the absence of H6-G2P.

We have investigated the effect of adding increasing G*1*P to the H6-G2P pattern of cleavage. The 320-bp *Eco*RI-*Pst*I SPP1 *pac* DNA segment (1 nM) was incubated with a constant amount of H6-G2P and various amounts of G*1*P (ratios: 1:0.25, 1:0.5, 1:1, 1:5, 1:10, and 1:50). At low G*1*P concentration, the H6-G2P cleavage pattern is similar to the one reported in Fig. 3*B*, and at higher G*1*P concentrations (>1:5) an inhibition of the nicking reaction was observed (data not shown). It is like that when decameric G*1*P was in a molar ratio of 1:5 or greater, the DNA is unavailable for H6-G2P cleavage. Alternatively, G*1*P exerts an inhibitory effect of H6-G2P endonuclease activity (see below).

H6-G2P Introduces Discrete Cleavage on Structured pac-containing DNA—Previously, we have shown that distamycin A (Dis), a minor groove binder that induces local distortions of the DNA, competes with G*1*P for *pac*L DNA binding, whereas other minor groove binders, such as spermine or Hoechst 33258, which do not distort DNA, failed to compete with G*1*P for *pac*L DNA binding (26). It was proposed that Dis mimics the DNA structure promoted by G*1*P upon binding to *pac* DNA (11, 26).

The 311-bp *Eco*RI-*Pst*I SF6 *pac* DNA segment (1 nM), labeled at the top strand, was preincubated with either 1 μM (Fig. 4*B*) or 100 μM Dis (Fig. 4*C*) for 20 min at room temperature and then incubated with increasing concentrations of H6-G2P. The resulting products were then separated in 6% denaturing PAGE. In the presence of 1 μM Dis, a DNA fragment ending at the *Y* site was not observed (Fig. 4*B*, *lanes 8–11*), when compared with the cleavage products generated by H6-G2P (40 nM) in the absence of Dis (Fig. 4*B*, *lane 7*). In the presence of the 100 μM Dis, only five DNA fragments ending at sites *3*, *2*, *4*, *1*, and *A* were observed. The DNA fragments ending at site 1 (5′-GCGG ↓ CA-3′) coincided with the *bona fide* terminase packaging initiation site (9, Fig. 4*C*). H6-G2P also introduced a nick at the second Box b site (5′-GCGG ↓ CA-3′, site 2). In the presence of 100 μM Dis, the DNA fragments ending at positions 3, 4, and A co-migrate with the DNA bands observed in the absence of H6-G2P (Fig. 4*C*, *lanes 12* and *14*). It is likely that: (i) H6-G2P recognized the sequence 5′-RCGG ↓ CW-3′ and preferentially cleaved the 5′-GCGG ↓ CA-3′ sequence embedded in a special architecture, and (ii) the repertoire of DNA structures generated by Dis partially mimicked the ones generated by G*1*P.

Dis Enhances H6-G2P Double Strand Cleavage within pacC—SPP1 399-bp *pac* DNA (5 nM), labeled at the bottom strand (see Fig. 5*A*), was preincubated with increasing concen-

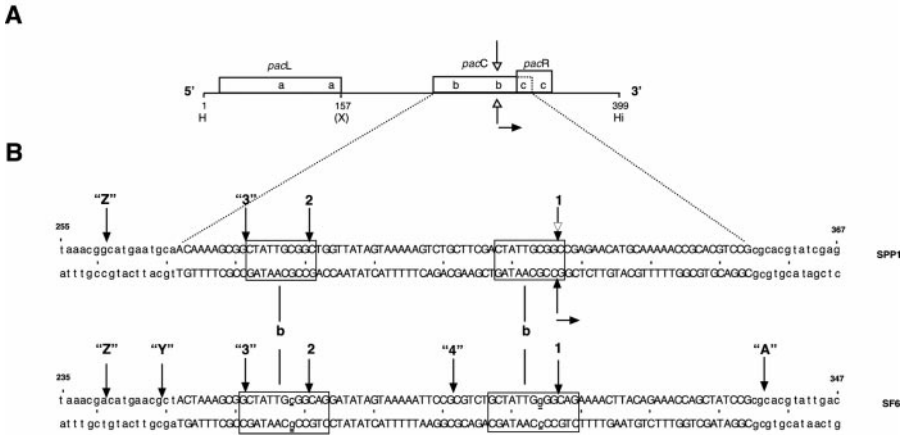

FIG. 3. **Scheme of H6-G2P cleavage sites.** *A*, a schematic representation of the SPP1 *pac* site. The *pac* region is subdivided into three discrete subsites (*pac*L, *pac*C, and *pac*R). The 100-bp *pac*L contains the two directly repeated 7-bp Box a sites, the 83-bp *pac*C site contains two directly repeated 10-bp Box b sites, and the 31-bp *pac*R contains two directly repeated 7-bp Box c sites. The *pac*C and *pac*R subsites partially overlap. The *in vivo pac*C cleavage site is indicated by *vertical arrows*, and the direction of DNA packaging is denoted by a *horizontal arrow*. The relevant restrictions sites are indicated. Abbreviations: *H*, *Hpa*II; *Hi*, *Hin*fI; *X*, *Xho*II. The parenthesis denotes that the *Xho*II site is not present in the wt phage DNA sequence. *B*, the nucleotide sequences of the 83-bp *pac*C site of both SPP1 and SF6 phages are indicated in *capital letters*. The 1-bp difference between the two directly repeated 13-bp Box b sites of phage SF6 is *underlined* and in *lowercase letters*. The *open arrows* denote the *bona fide pac*C cleavage, and the *solid arrows* indicate the H6-G2P nicks.

trations of Dis and then incubated with H6-G2P. The resulting products were then separated in a 4% non-denaturing PAGE. Previously, it was shown that the presence of increasing concentrations of Dis modified the mobility of SPP1 *pac* DNA (26, Fig. 5*B*, *lanes 3–6*). As revealed in Fig. 5*B*, H6-G2P cleaved a small fraction of the 399-bp SPP1 *pac* DNA to produce two dsDNA fragments of ~326 and ~291 bp (Fig. 5*B*). In the presence of 100 μM Dis, H6-G2P showed a marked preference to produce the 326-bp segment (Fig. 5*B*, *lane 3*). A nucleotide sequence analysis of the ends of those two dsDNA fragments showed that the double strand cleavage took place within the two 10-bp Box b sequences (3′-GATAACGCC ↓ Gg-5′ (site 1) and 3′-GATAACGCC ↓ Ga-5′ (site 2)) (Figs. 3*B* and 6*B*).

H6-G2P Hydrolyzes ATP—H6-G2P has a putative nucleotide-binding motif (8, 18). To determine whether H6-G2P is able to display an adenosine triphosphatase (ATPase) activity we measured ATP hydrolysis in the presence or absence of *pac*-containing DNA (pBT363) (1 nM). H6-G2P (20 nM) was able to hydrolyze the [γ-^{32}P]rATP or -dATP present in the reaction to rADP or dADP and P_i (data not shown). The rATP behaved as a Michaelis-Menten type substrate with the kinetic parameters of K_m = 994 ± 60 μM, k_{cat} = 27 min^{-1}, V_{max} = 0.54 ± 0.02 μmol min^{-1} mg^{-1} of H6-G2P (Fig. 6; data not shown). Such an ATPase activity was slightly increased by the addition of DNA (1.8-fold), but it was not affected by the presence of *pac*C-containing dsDNA or ssDNA linear DNA (data not shown).

Previously, it had been reported that G*1*P is unable to hydrolyze ATP (14, 15, data not shown). The effect of G*1*P on the ATPase activity of H6-G2P was investigated. The rate of H6-G2P-catalyzed ATP hydrolysis, in the presence of an optimal concentration of G*1*P (95 nM), as a function of ATP concentration is shown in Fig. 6. In the presence of G*1*P, H6-G2P (20 nM) was more active, with a K_m = 386 ± 50 μM, k_{cat} = 90 min^{-1}, V_{max} = 1.8 ± 0.05 μmol min^{-1} mg^{-1} of H6-G2P (see Fig. 6). Identical results were observed when wt G*1*P was replaced by G*1*PΔC136 (lacking the last 47 residues, domain III; see Fig. 7).

Like the endonuclease activity of the enzyme (see above), the ATPase activity exhibits an optimum at pH 7.8 and is inhibited by the addition of EDTA or when Mg^{2+} is replaced by Ca^{2+} or Zn^{2+} (<5% of the ATPase activity). When Mn^{2+} (10 mM $MnCl_2$) was used instead of Mg^{2+}, ~55% of the H6-G2P ATPase activity was detected.

G2P is able to hydrolyze [γ-^{32}P]rATP or [γ-^{32}P]dATP but fails to hydrolyze the remaining rNTPs and dNTPs (data not shown).

G1P Interacts with H6-G2P—Previously, it has been shown that H6-G2P interacts with wt G*1*P and G*1*PΔC136 but fails to interact with G*1*PΔN62 (lacking the first 62 residues, domain I) when polyclonal antibodies raised against purified G*1*P or G*1*PΔN62 immobilized in a protein A-Sepharose column were used (15). Using affinity chromatography (the protein cross-linked to a gel matrix (Affi-Gel, Bio-Rad) or the His-tagged protein metal chelated to the column) and protein:protein cross-linking, we confirmed that H6-G2P interacts with wt G*1*P and G*1*PΔC136 and showed that H6-G2P has a weak interaction with G*1*PΔN62, H6-G*1*PΔC55 (containing the first 54 residues, domain I) and H6-G*1*PN64-C141 (containing from residue 65 to 141, domain II) (18, Fig. 7*B*).

Using protein cross-linking techniques, we failed to detect a direct H6-G2P:H6-G2P interaction (Fig. 7*B*). The molecular mass of native H6-G2P, deduced from the amino acid sequence as 49,771 kDa, was then determined by gel filtration chromatography. From the elution profile of H6-G2P and of a number of protein standards, we estimate that the M_r of H6-G2P is ~50,000. The single H6-G2P peak in the chromatogram coincided with the eluted ATPase activity (data not shown). It is likely, therefore that H6-G2P is a monomer in solution.

In the previous section we showed that wt G*1*P stimulated ~3.5-fold the ATPase activity of H6-G2P. Alternatively, in the presence of H6-G2P, a cryptic ATPase activity associated with G*1*P could be detected. To address this question, different variants of G*1*P were incubated with H6-G2P and its ATPase activity measured. When G*1*PΔ62, which lacks the putative Walker's motif B (8, 18, Fig. 7), was incubated with H6-G2P, the H6-G2P ATPase activity was stimulated ~1.9-fold. The addition of G*1*PΔC55 (domain I containing Walker's motif B) (18), G*1*PN64-C141 (domain II containing the putative ADP and/or ATP-binding loop, Walker's motif A), or both proteins together, however, exerted a negative effect in the H6-G2P ATPase activity. (H6-G2P retained ~34% of its ATPase activity in the presence of H6-G*1*PΔC55, no activity was detected with H6-G*1*PN64-C141, or ~10% of the H6-G2P ATPase activity was detected in the presence of both H6-G*1*PΔC55 and H6-G*1*PN64-C141 polypeptides.)

The Amount of G1P Alters the Relative Activities of H6-G2P—In a previous section we showed that the presence of

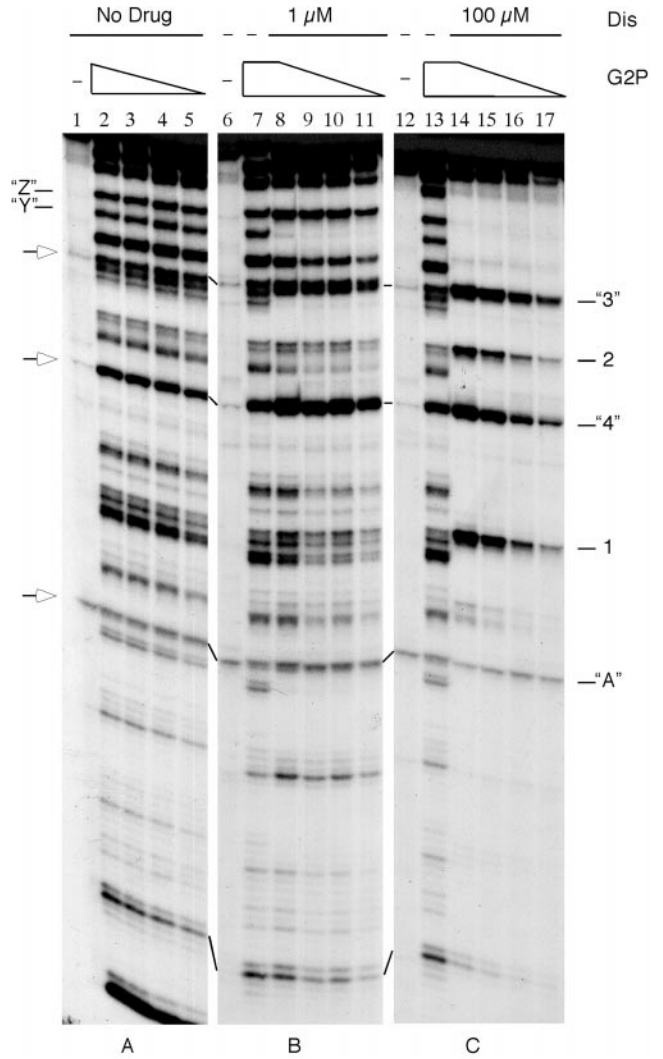

FIG. 4. **Nicking of *pac*-containing DNA by H6-G2P.** The α-^{32}P-labeled, 311-bp *Eco*RI-*Pst*I DNA segment (containing the 233-bp *Ear*I-*Hin*fI *pac* site of phage SF6 (coordinates 223–456, labeled in the top strand)) (1 nM in molecules) was resuspended in buffer B containing 10 mM $MgCl_2$, brought to 37 °C in a final volume of 20 μl and incubated in the absence (*A*) or the presence of 1 μM (*B*) and 100 μM (*C*) Dis. Then increasing concentrations of H6-G2P were added to the reaction, and incubation continued for 60 min. The reactions were terminated by the addition of EDTA, the resulting products were separated on a 6% denaturing PAGE, and the dried gel was autoradiographed. *Lanes 2*, *7*, *8*, *13*, and *14* contain 40 nM H6-G2P; *lanes 3*, *9*, and *15* contain 20 nM; *lanes 4*, *10*, and *16* contain 10 nM; and *lanes 5*, *11*, and *17* contain 5 nM H6-G2P. In *lanes 1–7*, *12*, and *13*, Dis was not added. In *lanes 1*, *6*, and *12*, H6-G2P was not added. In the DNA fragments (*1* and *2*) cleavage occurred at the two Box b sites, in the DNA fragments (*3* and *4*) the nick occurred within *pac*C but outside the two Box b sites, and the DNA segments ending at *Z*, *Y*, and *A* map outside *pac*C. *Arrows* denote DNA segments in the absence of H6-G2P.

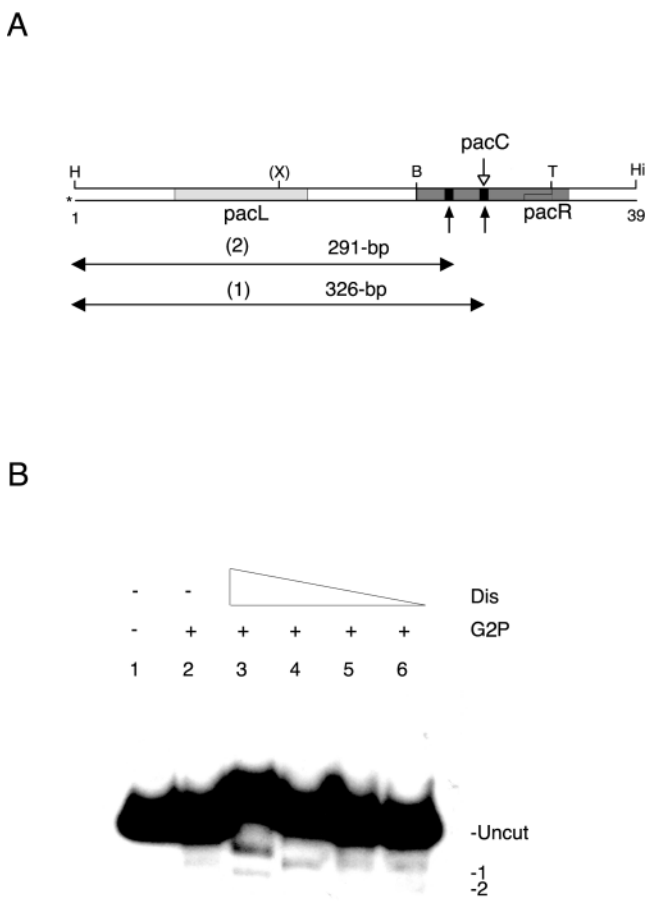

FIG. 5. **Nicking of both strands at Box b by H6-G2P in the presence of Dis.** *A*, physical map of the 399-bp SPP1 *pac* DNA. The *lines* represent the DNA, the *shaded area* denotes *pac*C, and the *black boxes* show the position of the Box b. The *pac*L (*dotted*) and *pac*R (*patched*) subsites are indicated. The *open arrows* denote the *bona fide pac*C cleavage, and the *solid arrows* the H6-G2P-generated ends. Abbreviations: *B*, *Bsm*I; *H*, *Hpa*II; *Hi*, *Hin*fI; *T*, *Tha*I; *X*, *Xho*II. Cleavage at the 10-bp Box b produced fragments of 326 bp (cleavage at site 1) and 291 bp (cleavage at site 2). The *asterisk* denotes the position of the radiolabeled end. *B*, the α-^{32}P-labeled 399-bp SPP1 *pac* DNA (1 nM) was preincubated with increasing concentrations of Dis (1, 10, 50, and 100 μM) in buffer B containing 10 mM $MgCl_2$ and was brought to 37 °C in a final volume of 20 μl. The reaction was then incubated with H6-G2P (20 nM), and the incubation was continued for 60 min. The reaction products were separated on a 5% non-denaturing PAGE. *Lane 1*, no protein, no Dis; *lanes 2–6*, 20 nM of H6-G2P; *lanes 3–6*, decreasing concentrations of Dis (100, 50, 10, and 1 μM).

increasing concentrations of G*1*P stimulated the ATPase activity of H6-G2P, but G*1*P might exert a negative effect on the H6-G2P endonuclease activity. We have investigated the effect of increasing amounts of G*1*P on the ATPase and endonuclease activities of H6-G2P. For the measurement of the *in vitro* endonuclease activity of H6-G2P, we used form I pBT363 DNA and measured the generation of form II and form III DNA. H6-G2P was incubated with increasing concentrations of G*1*P and then with supercoiled *pac*-containing pBT163 DNA. The ATPase activity was assayed as follows: H6-G2P was incubated with increasing concentrations of G*1*P and then with pBT363 DNA and 2.5 mM [γ-^{32}P]ATP. An identical ATPase activity was observed when DNA was omitted from the reaction mixture.

In the presence of 2 G*1*P decamers per H6-G2P monomer, a 1.8-fold reduction of the endonuclease activity (measured as the accumulation of form II and form III DNA) with a concomitant stimulation of its ATPase activity was observed (Fig. 8). In the presence of 4–12 G*1*P decamers per H6-G2P monomer, G*1*P fully stimulated the ATPase activity and drastically reduced the H6-G2P endonuclease activity (Fig. 8). The inhibitory effect of G*1*P in the endonuclease and stimulatory effect on the ATPase activity of H6-G2P were fully reversible (data not shown). It is likely, therefore, that G*1*P modulated the G2P activities.

DISCUSSION

The mechanism of site-specific packaging, in which the recognition sequence plays an important role in initiation and termination of packaging, has been well characterized (1–6). The mechanism of headful packaging, in which the packaging initiates at a specific site (*pac*) but with the capacity of the prohead playing a predominant role in the termination, is

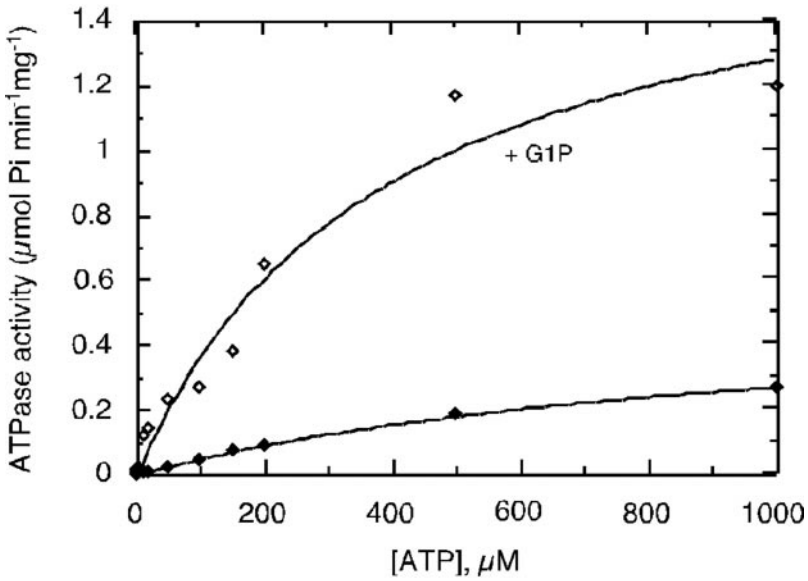

FIG. 6. **Kinetic analysis of the ATPase activity of H6-G2P and terminase by initial velocity *versus* substrate concentration.** The reaction conditions were as described under "Experimental Procedures." Each point represents the average of experiments done at least in triplicate. Kinetic parameters were obtained from the fitting of the experimental data to the Michaelis-Menten equation. The ATPase activity of H6-G2P (◆) and SPP1 terminase (◇) are indicated.

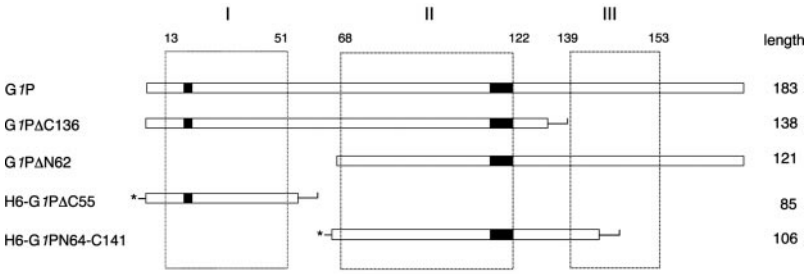

Protein	Interaction
H6-G2P	-
H6-G2P + G1P	++
H6-G2P + G1PΔC136	++
H6-G2P + G1PΔN62	+
H6-G2P + H6-G1PΔC55	+
H6-G2P + H6-G1PN64-C141	+

FIG. 7. **Schematic representation of SPP1 G*1*P.** wt G*1*P and deletion derivatives are shown as *solid boxes*. The *thin lines* denote non-G*1*P residues, and the *asterisks* indicate the hexa-histidine extension. Domains I (~39 residues in length), II (~56 residues), and III (~15 residues) are *boxed*. The polypeptide length is indicated. The putative Walker B nucleotide-binding motif and Walker A phosphate-binding loop (A*XXXX*GK(L/A)) are indicated as *solid boxes* in domains I and II, respectively. The physical interaction of H6-G2P with itself and with wt and the different variants of G*1*P is indicated. ++, denotes a positive interaction at 100 mM NaCl); + indicates a positive interaction at 25 mM, but a weak interaction at 100 mM NaCl; and −, no interaction.

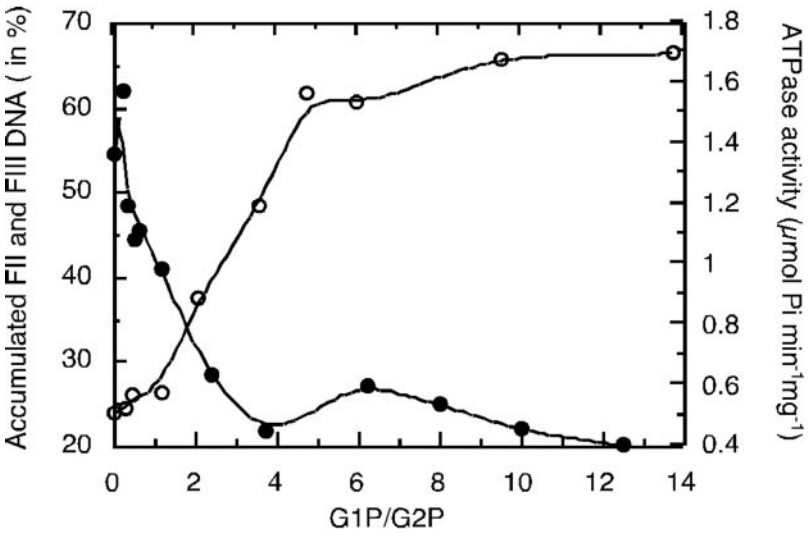

FIG. 8. **An increasing concentration of G*1*P stimulates the H6-G2P ATPase and exerts a negative effect on its endonuclease activity.** Supercoiled pCB363 DNA (20 nM in the endonuclease and 5 nM in the ATPase assay) was incubated with increasing concentrations of G*1*P (19, 28, 38, 47, 95, 190, 300, 500, 640, 800, and 1000 nM in the endonuclease and 5.1, 9.4, 23.7, 41.5, 71.4, 95, 119, 190, and 275 nM in the ATPase assay) and a constant amount of H6-G2P (80 nM endonuclease and 20 nM ATPase) in buffer B containing 10 mM $MgCl_2$ for 30 min at 37 °C. The percentage of relaxed plus linearized supercoiled *pac*-containing pBT163 DNA (●) and the ATPase activity of H6-G2P (○) are indicated.

poorly understood (1, 3, 7). The present study is our first step toward an understanding of terminally redundant and partially circularly permuted packaged molecules (headful packaging).

Previously we presented evidence that a plasmid-borne wt SPP1 gene *2* (G2P) or His-gene *2* (H6-G2P) fully complemented the amplification of SPP1 conditional lethal mutants in gene *2* (15). It is likely, therefore, that the addition of $(His)_6$ at the N

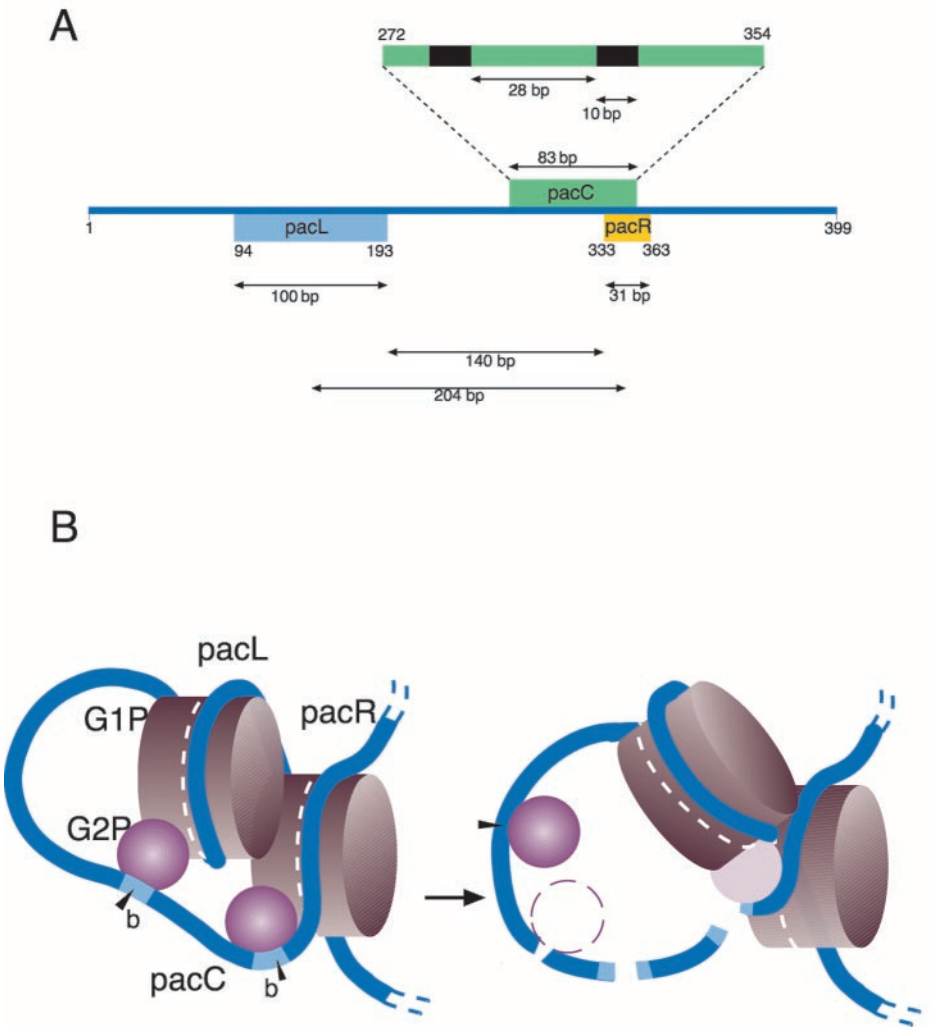

FIG. 9. **A model for headful packaging initiation.** *A*, the *pac* region is subdivided into three discrete subsites (*pac*L, *pac*C, and *pac*R). *pac*L is composed of a 100-bp region, *pac*C is composed of an 83-bp central region containing the two 10-bp Box b sites, and *pac*R is composed of a 31-bp region. *B*, the bead-like G*1*P particles bound to *pac*L and *pac*R might form a 204-bp loop containing the *pac*C subsite. G2P (*dark filled circle*, out of scale), possibly due to binding to G*1*P particles, binds and cleaves both Box b sites of *pac*C. The interaction of G*1*P bound to *pac*L with G2P:G*1*P-*pac*R induced a conformational change in this G2P molecule (*light filled circle*). The modified G2P has an increased ATPase activity and a reduced endonuclease activity. The G2P molecule freed of G*1*P at the *pac*L subsite (non-modified G2P) degraded the non-encapsidated DNA end. The *dotted empty circle* denotes a ghost G2P molecule after the introduction of a second or a third nonspecific cleavage. The *rightward pointing arrowhead* denotes endonucleolytic cleavage.

terminus of G2P does not affect the biological activity of the polypeptide. We have failed to overexpressed G2P or H6-G2P, but, taking advantage of affinity chromatography, we have purified H6-G2P from poorly expressing cells toward homogeneity (15). In this report we have biochemically characterized H6-G2P. H6-G2P possesses an endonuclease and ATPase that require Mg^{2+} and a neutral or slightly basic reaction pH. In the presence of Ca^{2+}, H6-G2P binds dsDNA rather nonspecifically but is unable to degrade DNA or to hydrolyze ATP.

Using a supercoiled DNA substrate, H6-G2P nicks and then linearizes DNA with poor sequence specificity. Using a linear DNA substrate and denaturing PAGE, we observed that the H6-G2P endonuclease showed a certain preference for the sequence 5′-RCGG↓CW-3′. The endonuclease activity and the cleavage specificity of H6-G2P were not stimulated by the presence of a nucleotide cofactor (ATP or dATP) or the presence of the DNA-bending Hbsu protein (5–400 nM) (*B. subtilis* counterpart of *E. coli* HU). A gene coding for the sequence-specific DNA-bending IHF protein cannot be identified in *B. subtilis*. Unlike the H6-G2P of SPP1, faithful cleavage of the P1 *pac* site requires phage-encoded terminase (PacA and PacB) and two *E. coli* chromatin-associated proteins (IHF and HU) (27). Furthermore, in the case of phage λ, the endonuclease activity of the terminase large subunit, gpA, is stimulated by the presence of the *E. coli* IHF protein (28, 29) and ATP (29, 30).

Previously we have shown that SPP1 G*1*P interacts with the *pac*L and *pac*R subsites and forms a loop that brings them together (11). Furthermore, Dis, which induces local distortions of the DNA, competes with G*1*P-*pac* complex formation (11, 26). When Dis was used instead of G*1*P, H6-G2P introduced ssDNA nicks and dsDNA breaks with high specificity at *pac*C. Our results suggest that Dis alters the conformation of *pac* DNA generating a repertoire of DNA structures that mimic the one generated by G*1*P. This is consistent with the fact that, in the presence of Dis, H6-G2P specifically nicks both DNA strands at the *bona fide pac*C subsite. Our results do not explain, however, how cleavage at other *pac*C subsites, except the one used for the initiation of DNA packaging, was prevented by the SPP1 terminase. In the P1 case Sternberg and coworkers (31) have shown that cleavage at the *pac* site is regulated by adenine methylation and that the P1 terminase "small" subunit (PacA) can discriminate between methylated and hemi- or unmethylated DNA, and accordingly, they proposed that *pac* cleavage is regulated by methylation of the DNA (27). Unlike P1, the SPP1 *pac* site does not contain DNA methylation sites for host DNA methyltransferases and SPP1 does not code for any DNA methyltransferase product (32).

Packaging of concatemeric DNA into a preformed prohead is believed to occur by a conserved mechanism, but certain details can vary from system to system. The terminase enzyme is directly involved in the initiation of packaging as well as in the ATP-driven translocation of DNA into a prohead (4–7). Previously we presented evidence that G*1*P binds but does not hydrolyze ATP (14). We show that H6-G2P hydrolyzes rATP and dATP to the corresponding diphosphate and inorganic phosphate with a low affinity for the nucleotide (K_m of 994 μM) and a k_{cat} of 27 min^{-1}. H6-G2P failed to hydrolyze the remaining rNTPs and dNTPs. ATP hydrolysis was marginally increased

by the addition of DNA (1.8-fold). Unlike SPP1 H6-G2P ATPase, the phage λ gpA ATPase is capable of hydrolyzing different nucleoside triphosphates (28, 29) and is active in the presence of Ca^{2+} as a divalent metal (29, 33). Both λ gpA (28, 29, 33) and H6-G2P (this work) display an *in vitro* ATPase activity independent of proheads, whereas such hydrolysis is dependent of proheads in the ϕ29, T3, and T7 packaging systems (see Ref. 6).

The presence of two to four molecules of G*1*P per H6-G2P molecule lowered the K_m (386 μM) and increased k_{cat} (90 min^{-1}) of H6-G2P ATPase ~3.5-fold, but the endonuclease was repressed. What could be the functional implications of the different stoichiometry of terminase on SPP1 headful packaging? G*1*P specifically binds, with high cooperativity, to two discrete (*pac*L and *pac*R) subsites, separated from each other by a stretch of 140-bp and bends the DNA (11, Fig. 9*A*). The interaction between a G*1*P decamer bound to *pac*L and a G*1*P decamer bound to *pac*R forms a specialized nucleoprotein structure that gives rise to a DNA loop of 204 bp in length (11, Fig. 9*B*). G*1*P interacts with H6-G2P (15, this work), and the H6-G2P target site (*pac*C) is located between the *pac*L and *pac*R subsites (8–10, Fig. 9). We show that the DNA architecture artificially generated by Dis stimulates the cleavage of H6-G2P to the *bona fide pac*C subsite and predict that the DNA distortion mediated by G*1*P could do so. G*1*P forms a nucleoprotein complex at the *pac*L and *pac*R subsites and interacts with G2P (11, 15). We hypothesize that the G*1*P-promoted architectural element facilitates the recognition and specific cleavage of G2P at both Box b sites as illustrated in a model presented in Fig. 9*B*. The interaction of two G*1*P decamers (bound to *pac*L and *pac*R) with G2P bound to the Box b proximal to *pac*R might induce a conformational change in G2P. "Modified G2P" has a stimulated ATPase with a shut off of nuclease activity, hence this DNA end is not degraded. G2P bound to Box b proximal to *pac*L, which is freed of G*1*P and not subjected to such a conformational change, degrades this DNA end that is not a substrate for encapsidation (Fig. 9*B*). We hypothesize that the overlapping of *pac*C and *pac*R might impart the unique directionally of packaging. The terminase, composed of 2 G*1*P and 1 G2P molecules, then participates in the translocation of the nondegraded DNA end into an empty prohead through a unique portal vertex structure of the prohead.

G*1*P, which is an abundant protein (16), bound to a second *pac* site in the concatemer, further stimulating the ATPase activity of "modified G2P." When the head becomes full, the speed of translocation could slow down and an "unknown signal" reversed modified G2P to its endonuclease form. When G2P finds a 5′-RGG ↓ CW-3′ site, it introduces a "headful" cut. In the absence of such a signal, the ATPase form of "G2P" remains active (translocase). The "conformational change" hypothesis is consistent with the biochemical data present here and with the previously published genetic data (8–10). In short, SPP1 encapsidates its DNA from concatemeric DNA molecules by a processive headful packaging mechanism. The *pac* site is used only once per packaging series, and the nonencapsidated *pac*C DNA end is subject to nucleolytic degradation. Furthermore, two different concatemeric plasmid molecules (each of them smaller in length than a mature SPP1 particle) could be encapsidated into a single SPP1 head before the headful signal is triggered and G2P endonuclease is activated (8–16, 34). We assume that the same hypothesis holds true for the highly related phage SF6 and that the same process is operative in other phages that package their DNA by a headful mechanism (see Refs. 35, 36).

Acknowledgments—We are very grateful to Thomas A. Trautner for his continuous interest in this project and to S. Chai for the communication of unpublished results.

REFERENCES

1. Casjens, S. (1985) *Virus Structure and Assembly* (Casjens, S., ed) pp. 75–147, Jones and Bartlett, Portola Valley, CA
2. Feiss, M. (1986) *Trends Genet.* **2,** 100–104
3. Black, L. W. (1989) *Annu. Rev. Microbiol.* **43,** 267–292
4. Murialdo, H. (1991) *Annu. Rev. Biochem.* **60,** 125–153
5. Catalano, C. E., Cue, D., and Feiss, M. (1995) *Mol. Microbiol.* **16,** 1075–1086
6. Fujisawa, H., and Morita, M. (1997) *Genes Cells* **2,** 537–545
7. Black, L. W. (1995) *Bioessays* **17,** 1025–1030
8. Chai, S., Bravo, A., Lüder, G., Nedlin, A., Trautner, T. A., and Alonso, J. C. (1992) *J. Mol. Biol.* **124,** 87–102
9. Deichelbohrer, I., Messer, W., and Trautner, T. A. (1982) *J. Virol.* **42,** 83–90
10. Bravo, A., Alonso, J. C., and Trautner, T. A. (1990) *Nucleic Acids Res.* **18,** 2881–2886
11. Chai, S., Lurz, R., and Alonso, J. C. (1995) *J. Mol. Biol.* **252,** 386–398
12. Tavares, P., Santos, M., Lurz, R., Morelli, G., de Lencastre, H., and Trautner, T. A. (1992) *J. Mol. Biol.* **225,** 81–92
13. Tavares, P., Lurz, R., Stiege, A., Rückert, B., and Trautner, T. A. (1996) *J. Mol. Biol.* **264,** 954–967
14. Chai, S., Kruft, V., and Alonso, J. C. (1994) *Virology* **202,** 930–939
15. Gual, A., and Alonso, J. C. (1998) *Virology* **242,** 279–287
16. Chai, S., Szepan, U., and Alonso, J. C. (1997) *Gene* **184,** 251–256
17. Lin, H., Simon, M., and Black, L. W. (1997) *J. Biol. Chem.* **272,** 3495–3501
18. Walker, J. E., Saraste, M., Runswick, M. J., and Gay, N. J. (1982) *EMBO J.* **1,** 945–951
19. Studier, F. W. (1991) *J. Mol. Biol.* **219,** 37–44
20. Sheridan, S. D., Benham, C. J., and Hatfield, G. W. (1998) *J. Biol. Chem.* **273,** 21298–21308
21. Sambrook, J., Maniatis, T., and Fritsch, E. F. (1989) *Molecular Cloning: A Laboratory Manual*, 2nd Ed., Cold Spring Harbor Laboratory, Cold Spring Harbor, NY
22. Alonso, J. C., Weise, F., and Rojo, F. (1995) *J. Biol. Chem.* **270,** 2938–2945
23. Gill, S. C., and von Hippel, P. H. (1989) *Anal. Biochem.* **182,** 319–326
24. Ayora, S., Rojo, F., Ogasawara, N., Nakai, S., and Alonso, J. C. (1996) *J. Mol. Biol.* **256,** 301–318
25. Scott, J. F., Eisenberg, S., Bertsch, L., and Kornberg, A. (1977) *Proc. Natl. Acad. Sci. U. S. A.* **74,** 193–197
26. Chai, S., and Alonso, J. C. (1996) *Nucleic Acids Res.* **24,** 282–288
27. Skorupski, N., Sauer, B., and Sternberg, N. (1994) *J. Mol. Biol.* **243,** 268–282
28. Tomka, M. A., and Catalano, C. E. (1993) *J. Biol. Chem.* **268,** 3056–3065
29. Rubinchik, S., Parris, W., and Gold, M. (1994) *J. Biol. Chem.* **269,** 13575–13585
30. Hwang, Y., and Feiss, M. (1996) *J. Mol. Biol.* **261,** 524–535
31. Sternberg, N., and Coulby, J. (1990) *Proc. Natl. Acad. Sci. U. S. A.* **87,** 8070–8074
32. Alonso, J. C., Lüder, G., Stiege, A. C., Chai, S., Weise, F., and Trautner, T. A. (1997) *Gene* **204,** 201–221
33. Tomka, M. A., and Catalano, C. E. (1993) *Biochemistry* **32,** 11992–11997
34. Alonso, J. C., Lüder, G., and Trautner, T. A. (1986) *EMBO J.* **5,** 3723–3728
35. Coren, J. S., Pierce, J. C., and Sternberg, N. (1995) *J. Mol. Biol.* **249,** 176–184
36. Leffers, G., and Rao, V. B. (1996) *J. Mol. Biol.* **258,** 839–850